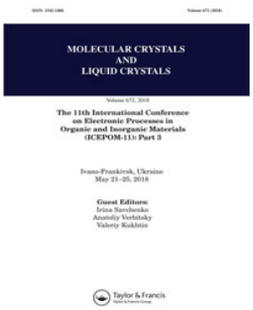

Molecular Crystals and Liquid Crystals

ISSN: 1542-1406 (Print) 1563-5287 (Online) Journal homepage: https://www.tandfonline.com/loi/gmcl20

Optical and electrical properties of β-Ni $(OH)_2$/ reduced graphene oxide nanocomposite

V. M. Boychuk, V. O. Kotsyubunsky, Kh. V. Bandura, A. B. Hrubiak, B. I. Rachii, I. P. Yaremiy & S. V. Fedorchenko

To cite this article: V. M. Boychuk, V. O. Kotsyubunsky, Kh. V. Bandura, A. B. Hrubiak, B. I. Rachii, I. P. Yaremiy & S. V. Fedorchenko (2018) Optical and electrical properties of β-Ni $(OH)_2$/ reduced graphene oxide nanocomposite, Molecular Crystals and Liquid Crystals, 672:1, 168-177, DOI: 10.1080/15421406.2018.1550589

To link to this article: https://doi.org/10.1080/15421406.2018.1550589

Published online: 13 Jun 2019.

MOLECULAR CRYSTALS AND LIQUID CRYSTALS
2018, VOL. 672, NO. 1, 168–177
https://doi.org/10.1080/15421406.2018.1550589

Optical and electrical properties of β-Ni $(OH)_2$/reduced graphene oxide nanocomposite

V. M. Boychuk[a], V. O. Kotsyubunsky[a], Kh. V. Bandura[a], A. B. Hrubiak[b], B. I. Rachii[a], I. P. Yaremiy[a], and S. V. Fedorchenko[a]

[a]Vasyl Stefanyk Precarpathian National University, 57 Shevchenko Str., Ivano - Frankivsk, 76025, Ukraine; [b]Institute of Metal Physics, National Academy of Science, 36 ACad.Vernadsky Boulevard, Kyiv, 03680, Ukraine

ABSTRACT

Structural and optical properties of β-Ni$(OH)_2$/reduced graphene oxide nanocomposite which was obtained by ultrasound dispersion of hydrothermally synthesized β-Ni$(OH)_2$ and reduced graphene oxide were investigated. Frequency dependencies of conductivity for initial components and composite materials were studied. Specific surface areas of reduced graphene oxide, β-Ni$(OH)_2$ and β-Ni$(OH)_2$/reduced graphene oxide are 402, 20 and 88 m^2/g, respectively. It was established that initial ultrafine β-Ni$(OH)_2$ and β-Ni$(OH)_2$/reduced graphene oxide composite have a percolation electrical conductivity. The enlarging of β-Ni$(OH)_2$/reduced graphene oxide optical direct band gap energy compared to the initial components due to O/C contents changes was observed.

KEYWORDS

Nickel hydroxide; reduced graphene oxide; ultrasound dispersion; hydrothermal synthesis

I. Introduction

Electrochemical supercapacitors with high specific power ($>10^4$ W/kg) take an intermediate position between lithium batteries and solid state or electrolytic capacitors [1]. Its operational principles are based on the electric double layer (EDL) formation on an electrode– electrolyte interface during polarization-induced charge separation processes. The extremely low effective thickness of EDL allows experimental achieving area-normalized capacitance values up to 4-5 $\mu F/cm^2$ for carbon-based electrodes [2]. For the case of carbon nanostructured materials with specific surface area in a range of 1000–3000 m^2/g the specific capacitance values of about 50-150 F/g depending on the electrolyte type (aqueous or organic) are typically reported [3]. At the same time their specific energy (0.1-5 Wh/kg) is too low for wide practical application. The using of both advantages of double-layer capacitance and charge storage based on fast Faradaic process at charge-transfer-reaction (so-called pseudocapacitance) allows to expand significantly the capabilities of such devices. The efficiency of charge storage mechanisms depends on properties of active electrode materials and for some successful combinations the specific capacitance value grows up to 1200 F/g [1]. The wide range of transitions metal oxides (MnO_2, Co_3O_4, NiO, Fe_3O_4, or V_2O_5) as well as their mixed oxides and hydroxides have been studied as a redox electrode for hybrid supercapacitors [4].

CONTACT V. M. Boychuk kotsuybynsky@gmail.com

The electron conductivity and fast redox surface process without phase transformations are the main preconditions of successful application of transition metals oxides and hydroxides as active materials of hybrid supercapacitors technology [5]. Nickel hydroxide β-$Ni(OH)_2$ is one of the promising electrode materials due to its low cost, non-toxicity and high redox activity. [6]. But its low electronic conductivity and large changes in volume during charge/discharge process are the main technological problems. The obtaining of nanocomposite materials based on nanostructured β-$Ni(OH)_2$ and carbon, in particular, graphene or reduced graphene oxide (rGO) is promising way of these problems solving [7]. Application of such systems allows reaching the extremely high values of specific capacity (about 1875 F/g) in water electrolytes with relatively high energy and power densities [8].

Te development of novel metal hydroxide/rGO hybrid materials for asymmetrical supercapacitors is an important step to high performance energy storage. At the same time, the problem of effective control of hybrid material electrical and electronic properties comes to the foreground because only in this case we can predict steps to the development of high performance device. Herewith finding the regularities between synthesis conditions and structural, morphological and also electrical conductivity of β-$Ni(OH)_2$/carbon composite is important for obtaining materials with predicted properties. This work is devoted to β-$Ni(OH)_2$/rGO nanocomposite obtaining and investigation.

II. Experimental details

Ultrafine β-$Ni(OH)_2$ was synthesized by hydrothermal treatment of sol obtained by interaction of $NiCl_2{\cdot}6H_2O$ and ammonia solutions with the presence of surfactant (polyethylene glycol 6000). The obtained precipitate was washed by distilled water (until pH =7) with further drying at 60 °C. Graphene oxide was obtained by standard Hummers method [9]. The reduction of graphene oxide was carrying out under the hydrothermal conditions with the presence of hydrazine hydrate [10]. β-$Ni(OH)_2$/rGO composite was obtained by ultrasound dispergation of β-$Ni(OH)_2$ and rGO in distilled water with β-$Ni(OH)_2$ and rGO with mass ratio of 2:1. Such a ratio was chosen for simultaneous obtaining of both high value of electrical conductivity and reactive ability of redox material.

Phase composition and crystalline structure of the synthesized materials were investigated by XRD (copper anode radiation, Bragg-Brentano scheme, DRON-3.0 diffractometer). The average size of coherent scattering domains (CSD) was calculated by Scherrer's formula. Particle's morphology was observed by SEM method (Vega 3 MLN TESCAN device). Porous structure and specific surface area were investigated by low-temperature nitrogen absorption (Quantachrome Autosorb Nova 2200e device). Optical absorption spectra (wavelength range of 200-600 nm) were obtained at room temperature (ULAB 102 UV spectrophotometer). The frequency dependence of electrical conductivity was investigated by impedance spectroscopy (Autolab PGSTAT 12/FRA- 2 device) in the frequency range of 0.01-100 kHz. The electrical conductivity was measured for cylindrical samples prepared by pressing at 60 kN. The narrow temperature interval of scan (293-333 K) was chosen taking into

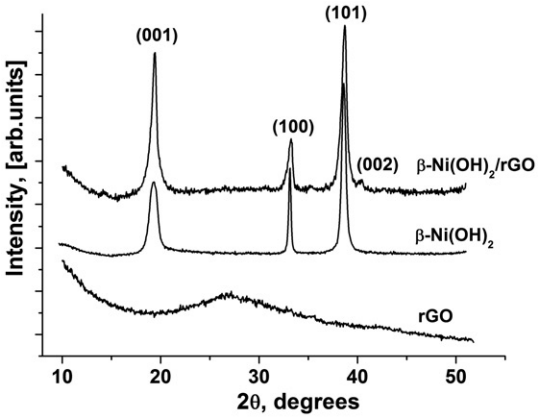

Figure 1. XRD patterns of rGO, β-Ni(OH)$_2$ and β-Ni(OH)$_2$/rGO.

account the probability of material thermal decomposition. The temperature control was carried out with accuracy of ±1 K.

III. Results

The initial rGO sample is close to amorphous and only diffuse galo is fixed on its XRD pattern in a range of $2\theta = 20–60^\circ$ (Fig. 1) due to crystalline structure disordering. The local maxima are observed at 27 and 42° that correspond to rGO structure [11]. XRD pattern of β-Ni(OH)$_2$ is characterized by broadening of (001) reflex due to the presence of nickel hydroxide particles with sizes about 30-40 lattice constants (15–20 nm) in the direction of C crystallographic axis. The presence of plane defects doesn't affect the width of this reflex [12]. These average crystallites sizes are about 15 nm. On XRD pattern of β-Ni (OH)$_2$/rGO composite the slight intensity increasing in the range of 25–30° is observed.

The broadening of (100) and (101) reflexes are observed which is caused by the presence of interpalanar defects. It can be assumed that ultrasonic dispersion led to the rGO fragments insertion into the interplanar space of β-Ni(OH)$_2$. The CSD average size of β-Ni(OH)$_2$ phase in composite material is about 13 nm.

According to SEM data initial rGO sample consists of graphene sheets packets while initial β-Ni(OH)$_2$ sample is formed by the spherical agglomerates with the sizes about 1-2 μm. Carbon fragments were observed between the agglomerated β-Ni(OH)$_2$ particles for composite material (Fig. 2).

Specific electric conductivity σ of the obtained materials was investigated at the temperature of 298, 303, 313, 323 and 333 K. $\sigma(\omega)$ curves are characterized by small changes at low frequencies and sharp increasing with the further frequencies enlarging that is typical for disordered materials with the hopping polaronic conductivity mechanism (Fig. 3a). According to [13] β-Ni(OH)$_2$ has protonic conductivity so carriers motion is determined by both charge transfer within grains and polarization effects on its border.

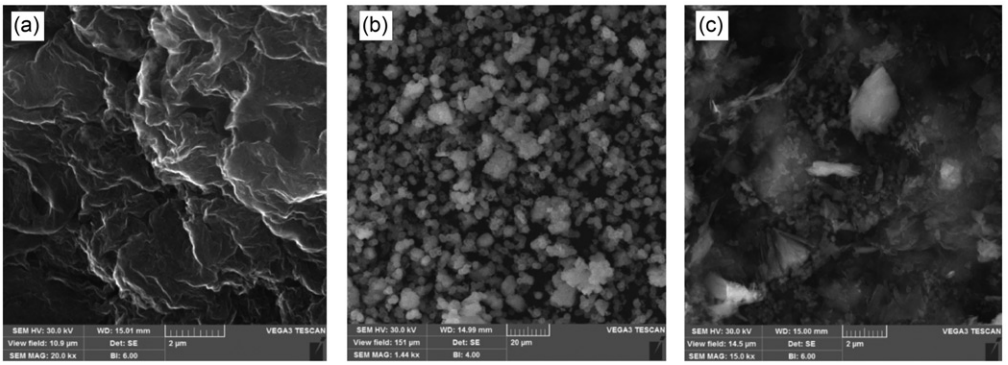

Figure 2. The SEM images of rGO (a), β-Ni(OH)$_2$(b) and β-Ni(OH)$_2$/rGO (c) particles.

The conductivity of the materials is the superposition of σ_{dc} (frequency independent component) and $\sigma_{\mathrm{AC}}(\omega)$ (polarized component) determined by percolation mechanism of charge transfer [14].

To describe this area Johnscher's model was used [15]. This model describe the charge transfer by electron percolation in the disordered potential under the electric field at the polarization effects: $\sigma_{AC}(\omega) = \sigma_{dc} + A\omega^n$, where σ_{dc} is the frequency independent conductivity, A is the dispersion parameter and n is the dimensionless frequency exponent which is a measure of the degree of interaction $0 < n < 1$ ($n = 0$ and 1 for an ideal Debye dielectric dipolar-type and $n = 1$ for an ideal ionic-type crystal). For β-Ni $(OH)_2$ sample n is 0.73 – 0.76 that indicates the diffusively limited character of carriers hops between adjacent quasi-equilibrium positions in the crystal separated by a potential barrier [16] and correlated barrier hopping mechanism of conductivity [17]. The expected temperature dependence of average hopping frequency ω_{h} (calculated as $\omega_h = \left(\frac{\sigma_{dc}}{A}\right)^{1/n}$) is $\omega_h = \omega_{dc} \exp\left(-\frac{E_h}{kT}\right)$. For β-Ni$(OH)_2$ the sharp increase in hopping frequency (from 220 to 510 s^{-1}) with temperature increasing to 303 K was observed with further decreasing to 110 s^{-1} at the 333 K (Fig. 4). The activation energy of electric conductivity (0.439 ± 0.020 eV) was calculated from Arrhenius plot for ultrafine β-Ni$(OH)_2$ sample. It is close to the activation energy value of about 0.485 ± 0.027 eV obtained using temperature dependence of the specific conductivity as follows $\sigma_{dc} = \frac{\sigma_0}{T} \exp\left[\frac{E_{\sigma_{dc}}}{kT}\right]$. The electrical properties of the rGO sample sharply change at relatively high frequencies (>1000 Hz) (Fig. 3b). The decreasing of material conductivity is explained by skin effect. The activation energy of electron traps in rGO is $(13.3 \pm 0.4) \cdot 10^{-3}$ eV. Frequency dependencies of the specific electric conductivity of β-Ni$(OH)_2$/rGO nanocomposite (Fig. 3c) were also approximated by universal power law. The systematic decreasing of conductivity σ_{dc} with the increasing of temperature was observed. The sharp increase in σ_{dc} and slightly decreasing of average hopping frequency ω_{h} for β-Ni$(OH)_2$/rGO sample compared to β-Ni$(OH)_2$ is observed. The hopping activation energy in percolation approach decreases to (0.099 ± 0.004) eV (Fig. 5).

Tauc model for the band gap energy E_g determination as a function of the incident photon energy was used. The absorption coefficient α near the band edge in semiconductors shows an exponential dependence accordingly to empirical relation $\alpha = \frac{const}{h\nu}[h\nu - E_g]^m$, where h – Planck's constant, ν – incident light wave frequency,

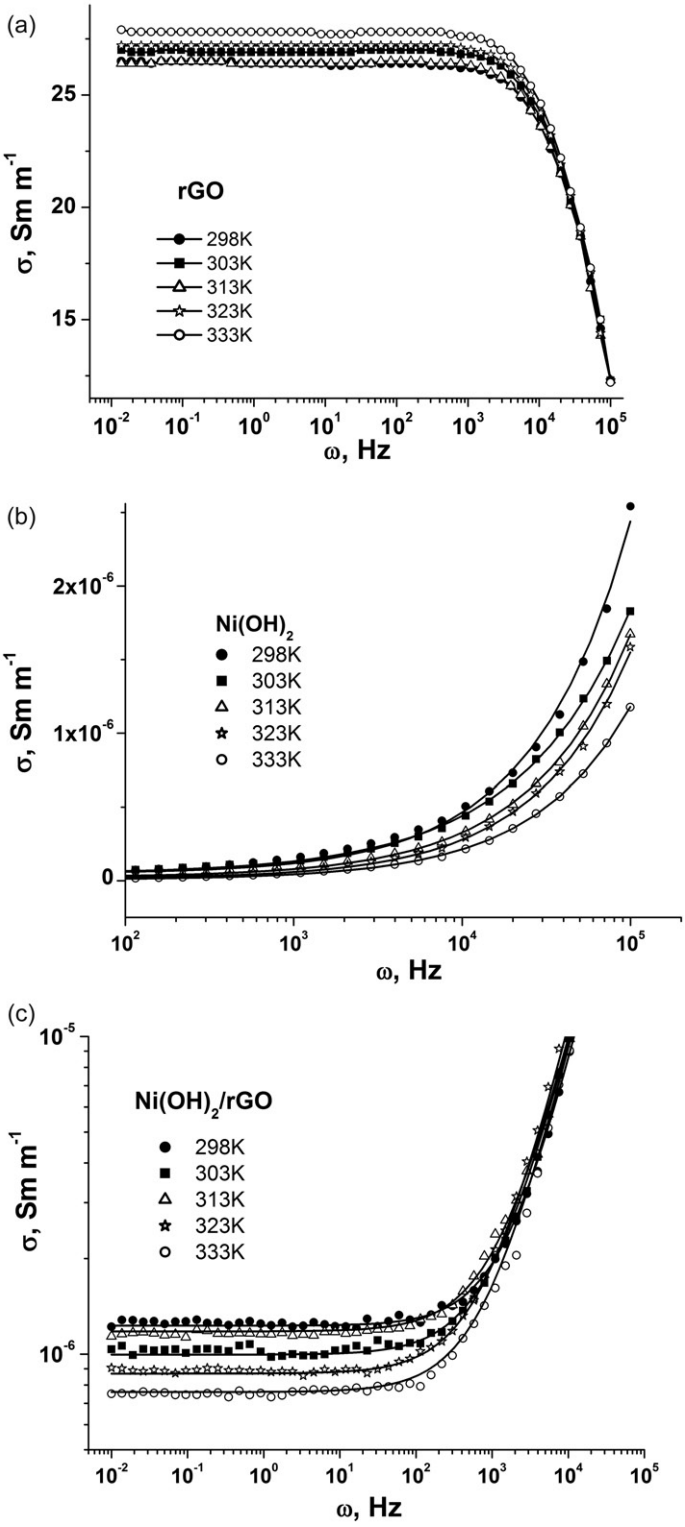

Figure 3. Frequency dependencies of specific conductivity rGO (a), β-$Ni(OH)_2$ (b) and β-$Ni(OH)_2$/rGO (c)

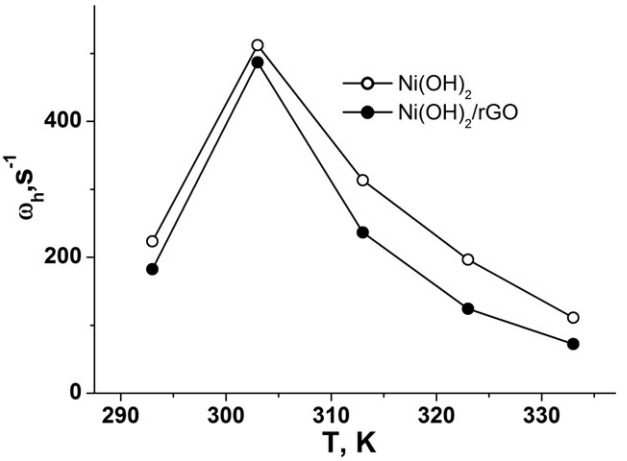

Figure 4. Temperature dependencies of the average frequency of hops of current carriers ω_h for β-Ni(OH)$_2$ and β-Ni(OH)$_2$/rGO nanocomposite.

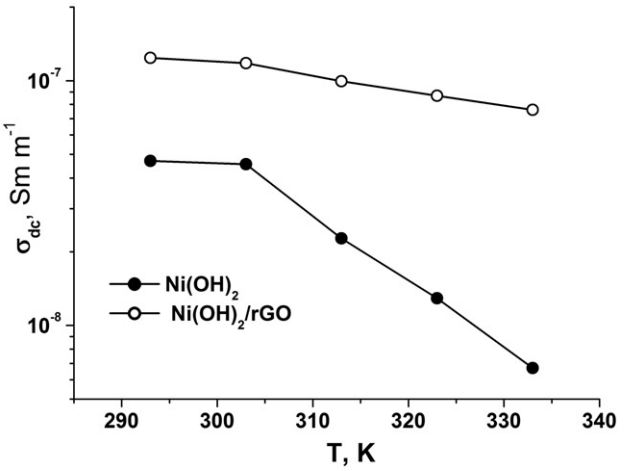

Figure 5. Temperature dependencies of the conductivity σ_{dc} of β-Ni(OH)$_2$ and β-Ni(OH)$_2$/rGO.

m = 1/2 and 2 for direct and indirect transitions, respectively. The extrapolation of the linear trend observed in the spectral dependence of $(\alpha h\nu)^2$ over a limited range of photon energies $h\nu$ was used and Tauc optical band gap is defined as occurring at the intercept of this linear extrapolation with the abscissa axis [18].

It was determined that direct-band optical transitions (m = 1/2) are typical for all the samples. The optical band gap energy for the β-Ni(OH)$_2$ sample is 3,80 ± 0,15 eV that corresponds to data of [19] obtained for nanocrystalline nickel hydroxide with average particle size of 22 nm. For microcrystal β-Ni(OH)$_2$ the direct optical band gap energy vary in a range of 3,0-3,5 eV [20]. An increasing of E_g can be associated with the quantum confinement effect [21].

The calculated value of the optical band gap energy for the rGO is 3.85 ± 0.12 eV sample that corresponds to [22] were hydrazine hydrate was used for graphene oxide reduction similar to our experiments. The estimated bandgap energy of rGO [23]

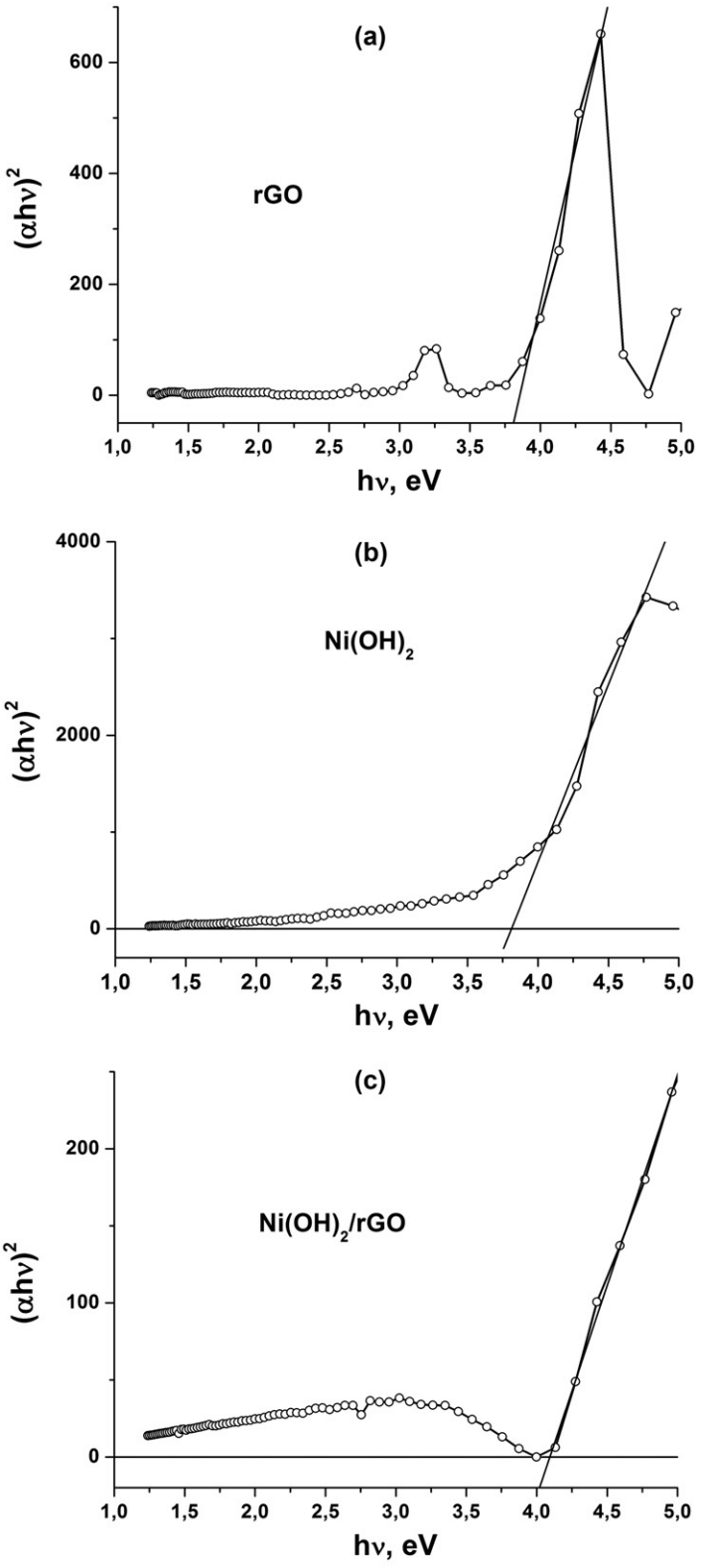

Figure 6. Tauc plots $(\alpha h\nu)^2(h\nu)$ of rGO (a), β-$Ni(OH)_2$ (b) and β-$Ni(OH)_2$/rGO (c).

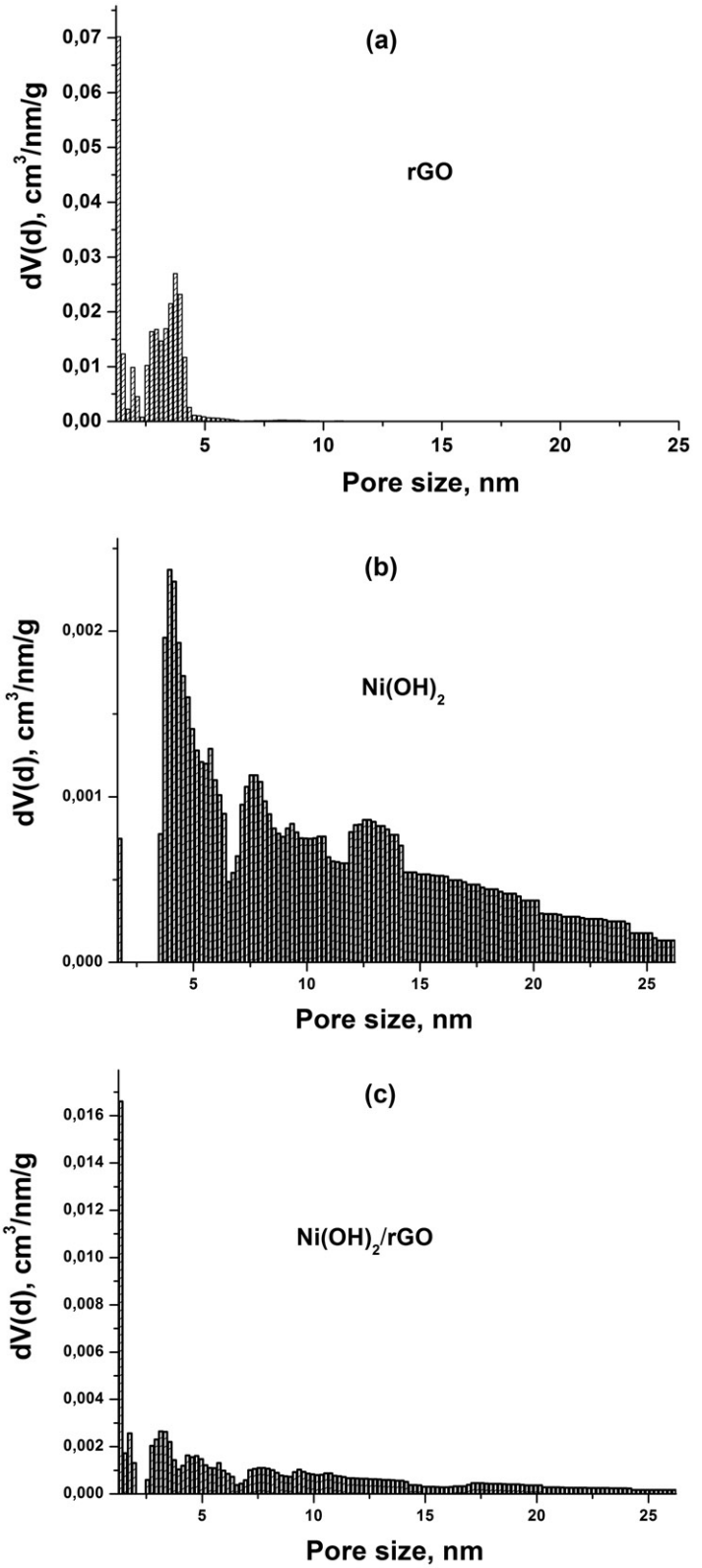

Figure 7. Pore sizes distributions for samples rGO (a), β-$Ni(OH)_2$ (b) and β-$Ni(OH)_2$/rGO (c).

depends on O/C ratio and enlarge with the oxygen density increasing. The integral value of band gap width of β-$Ni(OH)_2$/rGO composite is 4.09 ± 0.10 eV, i.e. there is an increase in both of the source material. The observed changes can be explained by peculiarities of composite forming. All obtained materials are characterized by a well-developed mesoporous structure (Fig. 7). At the same time the presence of micropores (up to 15% of total volume) is observed for β-$Ni(OH)_2$ sample, whereas for β-$Ni(OH)_2$/rGO composite pores of less than 2 nm are practically absent. Specific surface areas of rGO, β-$Ni(OH)_2$ and β-$Ni(OH)_2$/rGO are 402, 20 and 88 m^2/g, respectively. It can be assumed that ultrasonic treatment during the composite formation leads to with filling of the part of β-$Ni(OH)_2$ sample pores with graphene fragments. Herewith the increase of O/C ratio for the composite material may be expected that corresponds to the tendency of the optical bandgap energy increasing for rGO component. The using of aqueous medium during material preparation is the additional factor that causes an increase in the O/C ratio.

IV. Conclusions

β-$Ni(OH)_2$/rGO nanocomposite was obtained by ultrasonic dispergation hydrothermal synthesized β-$Ni(OH)_2$ and rGO in distilled water. The conductivity of both initial components and composite materials was investigated in percolation approach. Hopping conductivity is predominant for β-$Ni(OH)_2$ and β-$Ni(OH)_2$/rGO materials with activation energies of 0.485 ± 0.027 and 0.099 ± 0.004 eV, respectively. Average hopping frequency for β-$Ni(OH)_2$/rGO sample decreases compared to initial β-$Ni(OH)_2$. An electronic type of conductivity with activation energy of $(13.3 \pm 0.4) \cdot 10^{-3}$ eV for the reduced graphene oxide was observed. The formation of β-$Ni(OH)_2$/rGO nanocomposite leads to frequency-independent conductivity increasing and its temperature stability enlarging. The increase of the optical band gap energy of β-$Ni(OH)_2$/rGO nanocomposite (4.09 ± 0.10 eV) compared to the initial β-$Ni(OH)_2$ (3.80 ± 0.15 eV) and rGO (3.85 ± 0.12 eV) can be explained by the O/C ratio enlarging.

Acknowledgment

The work was carried out with the support of the Ministry of Education and Science of Ukraine, project 0116U007437.

References

[1] Simon, Patrice, and Yury Gogotsi. (2010). *Nanosci. Technol.*, 320–329.
[2] Ji H., Zhao X., Qiao Z., Jung J., Zhu Y., Lu Y., Ruoff R. S. (2014). *Nat. Commun.*, *5*, 3317.
[3] Inagaki, Michio, Hidetaka Konno, Osamu Tanaike (2010). *J. Power Sources*, *24*, 7880–7903.
[4] Dubal D. P., Ayyad O., Ruiz V., Gomez-Romero P. (2015). *Chem. Soc. Rev.*, *44*(7), 1777–1790.
[5] Wang G., Zhang L., Zhang J. (2012). *J. Chem. Soc. Rev.*, *4*, 797–828.
[6] Huang J., Xu P., Cao D., Zhou X., Yang S., Li Y., Wang G. (2014). *J. Power Sources*, *246*, 371–376.

[7] Wang H., Liang Y., Mirfakhrai T., Chen Z., Casalongue H. S., Dai H. (2011). *Nano Res.*, *4*(8), 729–736.
[8] Liu W., Ju C., Jiang D., Xu L., Mao H., Wang K. (2014). *Electrochimica Acta.*, *143*, 135–142.
[9] Marcano D. C., Kosynkin D. V., Berlin J. M., Sinitskii A., Sun Z., Slesarev A., Tour J. (2010). *M. ACS Nano*, *4*(8), 4806–4814.
[10] Long D., Li W., Ling L., Miyawaki J., Mochida I., Yoon. S. H. 2010. *Langmuir*, *26*, 16096–16102.
[11] Fu C., Zhao G., Zhang H., Li S. (2013). *Int. J. Electrochem. Sci.*, *8*, 6269–6280.
[12] Tessier C., Haumesser P. H., Bernard P., Delmas C. (1999). *J. Electrochem. Soc.*, *146*, 2059–2067.
[13] Deabate S., Henn F., Devautour S., Giuntini J. C. (2003). *J. Electrochem. Soc.*, *150*, J23–J31.
[14] Shyyko L., Kotsyubynsky V., Budzulyak I., Rachiy B. (2015). *Energetika*, *61*, 3-4.
[15] Jonscher A.K., (1996). *Universal Relaxation Law*. London: Chelsea Dielectric Press, UK.
[16] Mauritz K. A. (1989). *Macromolecules*, *22*, 4483–4488.
[17] Eilliot S.R. (1978). *Philos. Mag. B.*, *37*, 553–560.
[18] O'Learly S.K., Lim P.K. (1997). *Solid State Commun.*, *104*, 17–21.
[19] Shanaj B. R., John X. R. (2016). *J. Theor. Comput. Sci.*, *3*, 149.
[20] Hermet P., Gourrier L., Bantignies J. L., Ravot D., Michel T., Deabate S., Boulet P., Henn F. (2011). *Phys. Rev. B.*, *84*, 235211.
[21] Chukwuocha E. O., Onyeaju M. C., Harry T. S. (2012). *World J. Condens. Matter Phys.*, *2*, 96.
[22] Mathkar A., Tozier D., Cox P., Ong P., Galande C., Balakrishnan K., Ajayan P. M. (2012). *The Journal of Physical Chemistry Letters*, *3*, 986–991.
[23] Huang H., Li Z., She J., Wang W. (2012). *J. Appl. Phys.*, *111*, 054317.